ALTEX preprint
published January 27, 2020
doi:10.14573/altex.1909262

Research Article

An Advanced *In Vitro* Model to Assess Glaucoma Onset

*Sergio C. Saccà[1], Sara Tirendi[2,3], Sonia Scarfì[4], Mario Passalacqua[2], Francesco Oddone[5], Carlo E. Traverso[1,6], Stefania Vernazza[2,5 *] and Anna M. Bassi[2,3*]*

[1]IRCCS, San Martino General Hospital, Ophthalmology Unit, Genoa, Italy; [2]Department of Experimental Medicine (DIMES), University of Genoa, Genoa, Italy; [3]Inter-University Center for the Promotion of the 3Rs Principles in Teaching & Research (Centro 3R), Italy; [4]Department of Earth, Environmental and Life Sciences (DISTAV), University of Genoa, Genoa, Italy; [5]IRCCS, Fondazione G.B. Bietti, Rome, Italy; [6]Eye Clinic of Genoa, San Martino General Hospital, Department of Neuroscience, Rehabilitation, Ophthalmology, Genetics, Maternal and Child Health (DiNOGMI), University of Genoa, Genoa, Italy

Abstract

Glaucoma is the second leading cause of blindness worldwide. Currently glaucoma treatments aim to lower IOP by decreasing aqueous humor production or increasing aqueous humor outflow through pharmacological approaches or trabeculectomy.

However, the lack of effective cure requires new therapeutic strategies. In this regard, we compared the biological responses of a three-dimensional trabecular meshwork (TM) model with or w/o perfusion bioreactor technology to better understand the early molecular changes induced by prolonged oxidative stress condition. Therefore, we obtained standard 3D cultures from the embedment of TM cells in Matrigel and they were cultured both under static and dynamic conditions. In this regard, we demonstrated that the constant medium nutrients supply, conferred by perfusion bioreactor, improved the adaptive behavior to chronic oxidative stress of 3D TM cultures via offsetting pathway activation.

1 Introduction

Glaucoma is a neurodegenerative disease that involves 3.54% of the population aged 40-80 years (Tham et al., 2014). There are several types of this eye disease including primary open angle glaucoma (POAG), primary angle closure glaucoma, secondary glaucoma and developmental glaucoma. Whereas in POAG, a high-tension form of glaucoma, there is an increase in the intraocular pressure (IOP), in other forms of the disease, IOP is no longer considered the sole factor for the worsening of glaucoma, because its onset and progression can also occur within the normal IOP range (Kim and Park, 2019). Indeed, retinal ganglion cell (RGCs) death depends on a wide range of molecular events that underlie the pathogenesis of glaucoma and it is therefore crucial to further investigate the molecular mechanisms implied in RGCs apoptosis in order to counteract this process.

As known, the most common cause of the high-tension glaucoma cascade starts from the trabecular meshwork (TM), which is the first element of the conventional outflow pathway (Saccà et al., 2016b). In fact, since the TM is the most sensitive tissue to oxidative stress (OS), that is, damage caused in the anterior chamber of the eye (Izzotti et al., 2009), many different outcomes, such as TM mitochondrial dysfunction, inflammatory cytokine release, impairment of extracellular matrix (ECM) components and its turnover, cellular senescence promotion and a consequent loss of its cellularity, and so on, may occur (Zhao et al., 2016; Kim and Kim, 2018).

However, OS is also regarded to be the cause of pathological outcomes including ischemic, oxidative, inflammatory events which underlie glaucoma pathogenesis. Therefore, the resulting endothelial dysfunction which affects the endothelial cells of the trabecular meshwork occurs in both normal-tension glaucoma and high-tension glaucoma (Saccà et al., 2019).

Therefore, although the mechanisms by which the apoptotic signals develop towards retinal ganglion cells are not yet known, it has been hypothesized that the glaucomatous suffering of TM cells (TMCs), with or without the increase of IOP, affects their gene and protein expressions, generating molecular signals which, on reaching the head of the optic nerve, contribute to RGCs death (Saccà et al., 2016a).

Most of the studies carried out thus far to mimic different glaucomatous situations have referred to a variety of animal models (i.e. mouse, rat, rabbit, pig, cat, dog and monkey models). However, the obvious anatomical and morphological differences between animal and human eyes, together with the inflammation pathway triggered by the experimental approaches used to induce prolonged or transient elevation of intraocular pressure in animals, have necessitated an improvement of strategic approaches using human-specific models for glaucoma (Bouhenni et al., 2012; Langley et al., 2017).

There is therefore a growing interest for reliable 3D TM models as platforms for testing new therapeutics because, unlike 2D cell cultures, they mimic the true tissue nature in terms of morphology and environment (Brancato et al., 2018; Vernazza et al., 2019).

---

* contributed equally

Received September 26, 2019; Accepted January 23, 2020;
Epub January 27, 2020; © The Authors, 2020.

ALTEX 37(#), ###-###. doi:10.14573/altex.1909262

Correspondence: Stefania Vernazza, PhD,
Department of Experimental Medicine (DIMES)
University of Genoa
via L.B. Alberti 2, 16132 Genoa (Ge), Italy
(stefania.vernazza@yahoo.it)

In this regard, ex vivo models arising both from human and animal sources are the most widely used (Gonzalez et al., 2013; Li et al., 2019). However, their scarce availability reduces their use in perfusion studies and drug testing (Waduthanthri et al., 2019).

3D in vitro models could represent a good starting point to study several molecular features of glaucoma. Recently, natural polymer scaffolds such as collagen-chondroitin sulfate and matrix-based Matrigel® were used to study 3D-TM cell behavior under physiological and stress conditions (Bouchemi et al., 2017; Osmond et al., 2017).

The aim of the present study was to define a more realistic in vitro model to look at glaucoma onset and its outcomes by improving standard 3D-cultures performance. In this regard, we analyzed the pro inflammatory/pro apoptotic effects of chronic administration of hydrogen peroxide in Human Trabecular Meshwork Cells (HTMC) embedded in Matrigel® and cultured under both static and dynamic conditions. Given its biological composition based on basement membrane components (i.e. laminin, collagen IV, heparin sulfate proteoglycans and entactin), matrix degrading enzymes, their inhibitors, and numerous growth factors, Matrigel® was used to study the endothelial cell tube assay, 3D cancer cultures, the invasion assay, the organoid assembly, and the expansion of undifferentiated human embryonic stem cells (Kohen et al., 2009; Hughes et al., 2010; Benton et al., 2014). Most recently, the Matrigel® was also useful to mimic in vitro 3D-Trabecular Meshwork organization (Bouchemi et al., 2017; Vernazza et al., 2019). However, the innovation of our present work has been to improve the static culture conditions with a more complex 3D system capable of recapitulating distinct cell niches, under well-defined reproducible conditions such as chemical gradient supply (i.e. nutrients and oxygen). For this purpose, we applied millifluidic bioreactors technology to 3D-HTMC in vitro models, with the aim of allowing a continuous medium support in a constant flow rate without exposing the cells to a high shear force (Giusti et al., 2014; Berger et al., 2018).

2 Materials and Methods

Cell culture

HTMC and Trabecular Meshwork Growth Medium (TMGM) were acquired from Cell APPLICATION INC. (San Diego, CA, USA). Cell APPLICATION laboratory gave the official report on the evidence that the HTMC cells express several markers related specifically to a trabecular phenotype, since they resulted responsive to Dexamethasone treatment by increasing protein level expression of fibronectin, α-smooth muscle actin, myocilin and the cross-linked actin networks (CLAN)[1]. HTMCs were cultured according to consensus recommendations reported by Keller et al. (Keller et al., 2018) and were maintained at 37◦C in a humidified atmosphere containing 5% CO_2. All cell cultures were found to be mycoplasma-free during regular checks with the Reagent Set Mycoplasma Euroclone (Euroclone® Milan, Italy).

The 3D-cultures were performed as previously described by embedding HTMC into 100% Corning® Matrigel® Matrix (Corning Life Sciences, Tewksbury, MA USA) at density of $2*10^6/cm^3$ into and seeded directly in LiveBox1 (IVTech S.r.l. - Massarosa, Italy) bioreactor culture chamber, 1.7 cm^2 grow area/dish, (dx.doi.org/10.17504/protocols.io.574g9qw), in both static and flow conditions (Vernazza et al., 2019).

Dynamic 3D-HTMC system

To study 3D-HTMC behavior under dynamic conditions, we used a sophisticated model of milli-scaled multi-organ devices in a single flow configuration (LB1, IVTech srl) (Ucciferri et al., 2014). This device was composed of a peristaltic pump (LF, IVTech srl), transparent culture chambers, and a mixing bottle, all equipped with inlet and outlet pipes on the sides that allowed them to be interconnected. After seeding, each culture chamber containing the cells was filled with 1ml of culture media and placed in an incubator for 24hrs. The next day, 9 ml of culture media was put into a mixing bottle and by way of the peristaltic pump, the complete circuit was adequately filled to avoid any nutrient depletion. The culture medium circulated in this closed circuit at a constant flow rate of 70µL/min with basal perfusion. The flow rate was set to overcome both diffusional limitations and Matrigel® degradation over time (Fig. 1).

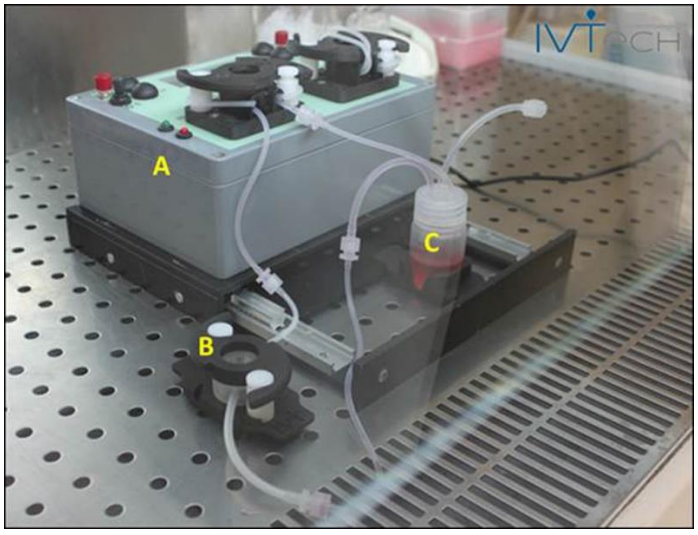

Fig. 1: Perfusion bioreactor circuit diagram
From the mixing bottle (C), the medium is pumped by the action of the peristaltic pump (A), through the perfusion chamber where 3D-HTMCs were seeded (B), then it returns to the medium reservoir, completing the circuit. The image represents only one circuit, but the flow system includes two head pumps connected with at least four perfusion chambers (kindly provided by IVTech srl).

[1] https://www.cellapplications.com/human-trabecular-meshwork-cells-htmc

Chronic stress condition

The prolonged oxidative stress effect in both 3D-models lasted for a week exposing once a day for 2 hours 3D-HTMCs to 500µM H_2O_2, followed by 22h of recovery, according to Poehlmann et al., 2013 and Kaczara et al., 2010 (Kaczara et al., 2010; Poehlmann et al., 2013). All molecular analyses on static and dynamic 3D-HTMC cultures were conducted once cells were freed from Corning® Matrigel® Matrix (Corning Life Sciences, Tewksbury, MA USA) by Corning Cell Recovery (Corning Life Sciences), according to the manufacturer's instructions.

Confocal analysis

At each selected check point time, the 3D-HTMCs, cultured and treated as mentioned above, were set in 4% paraformaldehyde and permeabilized with 0.3% Triton X-100 (Sigma Aldrich®, Milan, Italy). Nuclei were stained with To-Pro™ -3 Iodide 642/641 (Thermofisher Scientific Inc., Monza, Italy), actin cytoskeleton was visualized using Phalloidin Alexa Fluor 488 (Cell Signaling Technology, Danvers, USA). Fluorescence signals were captured at 60X magnification, by Leica TSC SP microscope (Leica Microsystem, Wetzlar, Germany); moreover, both fluorescence signals and F-actin intensity mensuration were elaborated by Fiji-ImageJ software, an open-source platform for biological-image analysis. Signals from different fluorescent probes were taken in sequential scan settings (3D reconstruction images).

Alamar Blue assay

The 3D-HTMC healthy state was daily carried out by AB assay (Invitrogen™, Thermo Fisher Scientific Inc., Monza, Italy) within the last 4 hrs of the 22hrs of recovery time, according to the manufacturer's instructions. In short, 10% (v/v) of AB solution was added to each well and, after 4 hrs of incubation, the resazurin reduction was quantified spectrophotometrically at wavelengths of 570 and 630 nm. The results were expressed as fold of reduction activity of treated vs untreated 3D-HTMCs.

RNA extraction, cDNA synthesis and qPCR analyses

3D-HTMCs (5×10^5) were treated as mentioned above and then a gene expression profile was obtained at 48hours by qPCR analysis and compared to control cells. Total RNA was extracted using the RNeasy Micro Kit (Qiagen, Milan, Italy) according to the manufacturer's instructions. NanoDrop spectrophotometer (Nanodrop Technologies, Wilmington, DE, USA) was used to quantify the RNA. Then, 150 ng per sample of cDNA was synthesized by using SuperScript™ III First Strand Synthesis System (ThermoFisher Scientific). Each PCR reaction was performed as described elsewhere (Vernazza et al., 2019). Values were normalized to ubiquitin (reference gene) mRNA expression. All primers (Tab. 1) were designed using the Beacon Designer 7.0 software (Premier Biosoft International, Palo Alto CA, USA) and obtained from TibMolBiol (Genova, Italy). Data analyses were obtained using the DNA Engine Opticon® 3 Real-Time Detection System Software program (3.03 version) and, in order to calculate the relative gene expression compared to an untreated (control) calibrator sample, the comparative threshold Ct method (Aarskog and Vedeler, 2000) was used within the Gene Expression Analysis for iCycler iQ Real Time Detection System software (Bio-Rad) (Vandesompele et al., 2002).

Human apoptosis array

Apoptosis was investigated by the semi-quantitative detection of 43 human apoptotic proteins, on customized Human Apoptosis Array C1 chip (RayBio®; Norcross, GA) (Tab. 2), according to the manufacturer's instructions. The intensity of protein array signals was analyzed using a BIORAD Geldoc 2000 and each protein spot was normalized against Positive Control Spots printed on each membrane.

The data analysis was conducted according to the Protocol directions of Human Apoptosis Array C1, and the relative protein expression on different arrays was extrapolated by using the algorithm, according to Human Apoptosis Array C1 protocol.

Tab. 1: Primer sequences used for real time quantitative polymerase chain reaction analysis

Gene	GenBank	Forward	Reverse
IL-1alpha	NM_000575.4	CAATCTGTGTCTCTGAGTATC	TCAACCGTCTCTTCTTCA
IL-1beta	NM_000576.2	TGATGGCTTATTACAGTGGCAATG	GTAGTGGTGGTCGGAGATTCG
IL-6	NM_001318095.1	CAGATTTGAGAGTAGTGAGGAAC	CGCAGAATGAGATGAGTTGTC
MMP-1	NM_001145938.1	GGTGATGAAGCAGCCCAGATG	CAGAGGTGTGACATTACTCCAGAG
MMP-3	NM_002422.5	TAATAATTCTTCACCTAAGTCTCT	AGATTCACGCTCAAGTTC
MMP-9	NM_004994.2	AACCAATCTCACCGACAGG	CGACTCTCCACGCATCTC
TNFα	NM_000594.4	GTGAGGAGGACGAACATC	GAGCCAGAAGAGGTTGAG
TGF-beta2	NM_001135599.3	AACCTCTAACCATTCTCTACTACA	CGTCGTCATCATCATTATCATCA
Ubiquitin C	NM_021009.7	ATTTGGGTCGCAGTTCTTG	TGCCTTGACATTCTCGATGGT
HPRT1	NM_000194.3	GGTCAGGCAGTATAATCCAAAG	TTCATTATAGTCAAGGGCATATCC

Tab. 2: The mini map of Human Apoptosis Array C1 (according to RayBio® manufacturer manual)

	A	B	C	D	E	F	G	H	I	J	K	L	M	N
1	POS	POS	NEG	NEG	Blank	Blank	bad	bax	Bcl2	Bcl2-w	BID	BIM	Caspase3	Caspase8
2														
3	CD40	CD40L	cIAP2	CytoC	DR6	Fas	FasL	Blank	Hsp27	Hsp60	Hsp70	HTRA2	IGF1	IGF2
4														
5	IGFBP1	IGFBP2	IGFBP3	IGFBP4	IGFBP5	IGFBP6	IGF-1R	Livin	P21	P27	P53	SMAC	Survivn	TNF RI
6														
7	TNF RII	TNFα	TNFβ	TRAIL R1	TRAIL R2	TRAIL R3	TRAIL R4	XIAP	Blank	Blank	NEG	NEG	POS	POS
8														

Western blotting

Total proteins were extracted from HTMCs as described elsewhere (Vernazza et al., 2019) and were resolved in Ani kD™ mini precast gel (Bio-Rad Laboratories, Inc., Hercules, CA, USA) in SDS-PAGE Running Buffer. Blots were incubated PARP1, phospho-NF-kB p65, Ser 536 (Cell Signaling Technology, Danvers, MA, USA) antibodies. To normalize each loading of the lanes, blots were stripped and incubated with GAPH antibody. The proteins were detected by Western Bright™ ECL (Advansta, CA, USA), exposed to film and analyzed using a BIORAD Geldoc 2000. Densitometrical data obtained from Quantity One software (Bio-Rad Laboratories, Inc., Hercules, CA, USA) were applied for statistical analysis and normalized against the housekeeping GAPDH. The results were expressed as fold vs untreated cultures, respectively.

Statistical analysis

Reported data are expressed as mean ± Standard Deviation (SD) and results were analyzed using two-way analysis of ANOVA for single comparison or two-way analysis of ANOVA variance followed by Bonferroni posttest for multiple comparisons. GraphPad Prism for Windows-version 5.03 and GraphPad Software, Inc., La Jolla, CA, USA) was used. Statistically significant differences were set at $p<0.05$; $p<0.01$; $p<0.001$.

3 Results

3.1 Alamar Blue assay

The effects of chronic 500µM H_2O_2 exposure were daily measured on 3D-HTMC cultures in static and dynamic conditions at each 24 hours check point time up to 168 hrs, by Alamar Blue assay (Fig. 2).

Over the first 24 hrs, the metabolic state of the 3D-static HTMC cultures showed a significant increase compared to the untreated cultures (about 50%), and the obtained levels in the following exposure times resulted in a time-dependent decrease. After 24-48 hrs of prolonged oxidative stress, the 3D-static HTMCs exhibited an increase of approximately 50 % in metabolic activity compared to the respective untreated cultures and 80% versus the 3D-dynamic HTMCs exposed to OS. These effects decreased slowly during the following time exposures, and at 96 hrs the metabolic rate resulted in being similar to that of control cultures. Over 120 hrs of prolonged stress conditions, HTMCs exhibited a further impairment of their metabolic state reaching lower values than those of the untreated cultures. Instead, the metabolic trend of 3D- dynamic HTMCs did not show a significant modulation within 24 hrs of applied stress. Nevertheless, repeated OS exposure produced a significant decrease in the viability index (about 20% vs untreated dynamic cultures), while remaining low up to 96 hrs, then a slow recovery of 3D-dynamic HTMCs was observed, starting from 144 hrs, resulting in a metabolic rate index similar to the control cultures.

3.2 qPCR

In order to evaluate the cytokines production, the MMPs regulation and ECM gene expression after OS treatment on 3D-HTMCs cultured in a static and dynamic manner, the cells were treated as mentioned above for 48h. The gene expression levels of IL-1α, IL-1β, IL6, TNFα, TGFβ, MMP1, MMP3, MMP9, COL1A1 and FN1 were analyzed by qPCR (Fig. 3). At 48h only OS-treated 3D-dynamic HTMCs showed an up-regulation of IL1β, TGFβ, MMP1, MMP3 and MMP9, compared both to untreated cultures and OS-treated 3D-static HTMCs.

However, OS-treated 3D-static HTMCs evidenced a significant increase only for IL1α levels compared both to untreated cultures and OS-treated 3D-dynamic HTMCs.

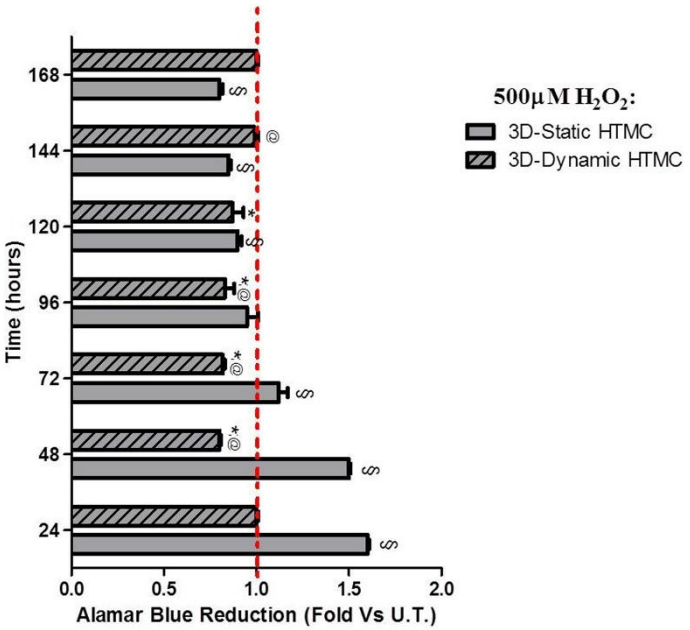

Fig. 2: HTMC metabolic state
Metabolic state of 3D HTMCs cultured in static and dynamic conditions was analyzed by Alamar blue assay, during the last 4 hrs of the 22 hrs recovery time in between daily exposure to oxidative stressor. The red dotted line represents the metabolic state of untreated (UT) 3D HTMCs cultured both in static and dynamic conditions, the gray bars represent the treated 3D HTMCs with 500µM H_2O_2. Data are expressed as "fold" Vs viability index of untreated 3D-HTMC, and each value represents the mean ± SD of 3 separate experiments running in triplicate. $^{*;§}p<0.001$ vs respective UT 3D-HTMCs; $^{@}p<0.001$ vs treated 3D-static HTMC (Two-way ANOVA followed by Bonferroni posttests).

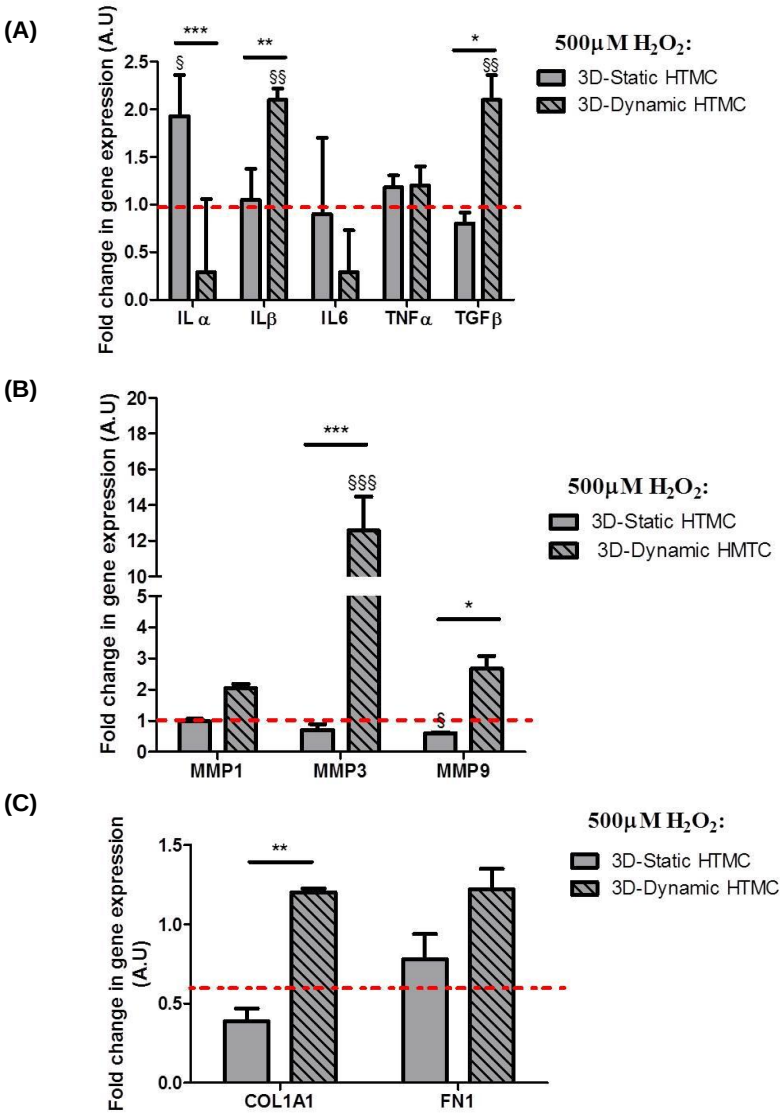

Fig. 3: Quantitative PCR gene expression analysis of 3D-HTMCs cultured in static and dynamic conditions and subjected to 500µM H_2O_2 for 48h

IL-1α, IL-1β, IL6, TNFα and TGFβ (A), MMP1, MMP3 and MMP9 (B), COL1A1 and FN1 (C). The red dotted line represents the gene expression of untreated (UT) 3D HTMCs cultured both in static and dynamic conditions, the gray bars represent the treated 3D HTMCs with 500µM H_2O_2. Data are expressed as fold-increase relative to control at the same end-point and normalized to Ubiquitin (Panels A-B) and HPRT1 (Panel C) housekeeping gene expression. Each bar represents the mean ± SD. of three independent experiments performed in triplicate.

$^{§}p<0.05$; $^{§§}p<0.01$; $^{§§§}p<0.001$ vs respective UT 3D-HTMCs; *p<0.05; **p<0.01; ***p <0.001 vs treated 3D-static HTMC (Two-way ANOVA followed by Bonferroni posttests).

3.3 Human apoptosis array

After prolonged OS stress, multiple marker detection of apoptosis pathway was analyzed on both 3D-HTMC models by a microarray for 43 pro/anti apoptotic proteins. In Fig. 4 we reported only the levels of those pro/anti-apoptotic proteins that resulted in significant modulation in almost one or in both 3D-HTMC models.

After 48 hrs OS exposure, 3D-static HTMCs evidenced a significant increase of pro-apoptotic BID, BIM, Caspase 3, p53, Smac, TNF-R1 proteins (Fig. 4A). This modulation resulted more marked after 72 hrs for above proteins, except for proapoptotic p53 and Smac. Regarding antiapoptotic molecules, the OS exposure after 48hrs resulted in a significant increase in Survivin, IGFBP1 and IGF1, and after 72 hrs, a stronger increase in BCL2, BCLw, survivin, x IAP, CD 40 and IGF1. These modulations of pro and anti-apoptotic markers are lapsed in 3D-static cultures at 168 hrs,

In dynamic conditions, after 48 hrs of OS stimulus, pro-apoptotic BAD, BID, BAX, BIM, CytoC, Smac and TNFα, TNFα/TNFR1, TNFα/TNFR2 protein levels were significantly increased compared to those of control cultures. At 72 hrs the levels of almost all markers were at basal levels, except for TNFα, TNFα/TNFR1, TNFα/TNFR2 which rose in a time dependent way until 168 hrs. As for anti-apoptotic patterns, only IGFBP1 evidenced a significant increase after 48 hrs, while BCL2, BCLw, Hsp70, CD40, IGFBP1 and IGF1 showed up to 3-fold increase after 168 hrs.

(A)

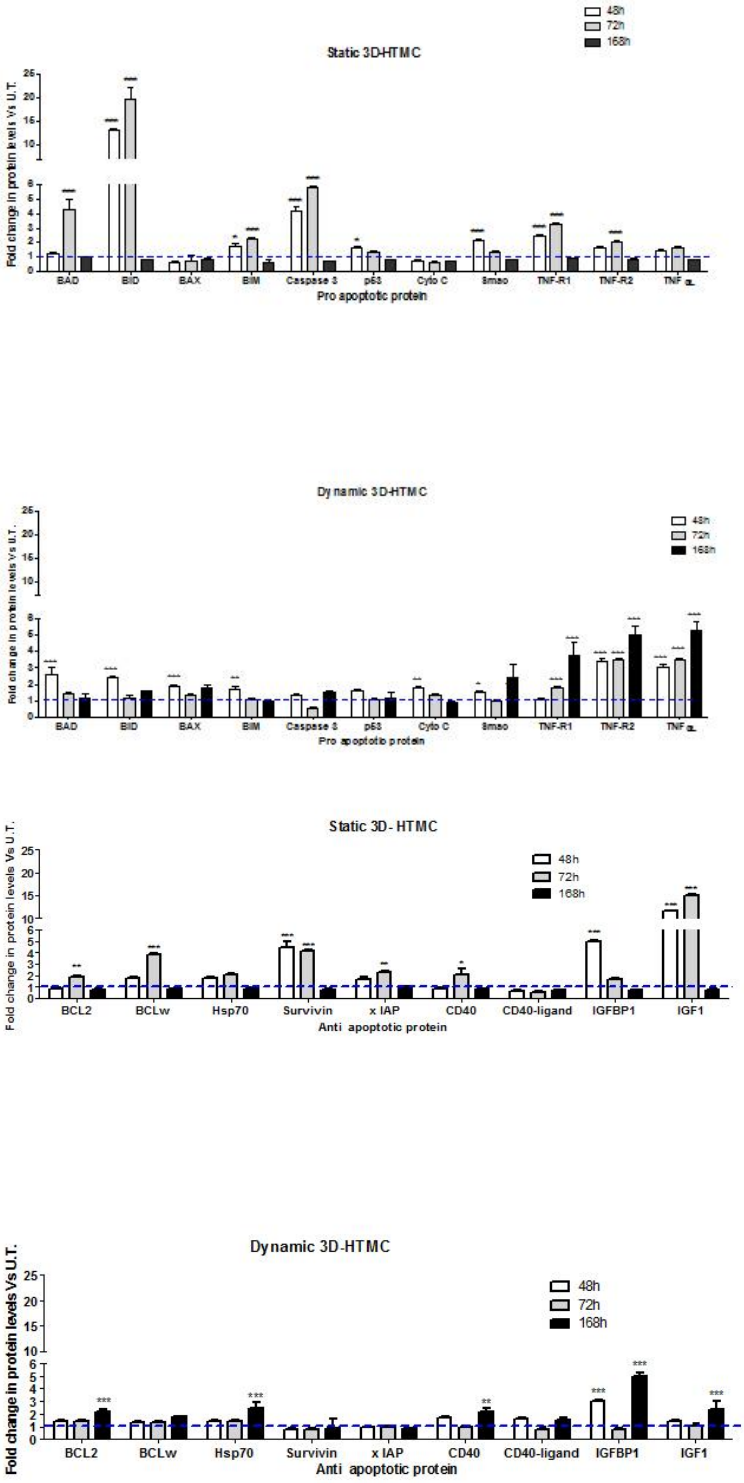

(B)

Fig. 4: Apoptosis array
Analysis of pro- and anti- apoptotic protein levels (Panel A and Panel B, respectively) in 3D-HTMCs cultured in static and dynamic conditions, were performed after 48-72-168hrs of 500µM H_2O_2, by Human Antibody Array C1 (RayBio® C-series). In the graphs only the analysis of the markers significantly modulated were reported. The light blue dotted line represents the protein level of untreated HTMC for each protein examined. Twelve individual models were arrayed (six static 3D-HTMCs plus six dynamic 3D-HTMC) and per experiment the intensity of Positive Control Spot was used to normalize signal responses for comparison of results across multiple arrays. *p<0.05; ** p<0.01; ***p<0.001 vs. respective untreated cultures (One-way ANOVA).

3.4 Western blot analysis

The analysis of PARP-1 full length-cleavage was performed on 3D-HTMCs, after 168 hours of exposure to chronic pro-oxidant stimulus (500µM H_2O_2) (Fig. 5). Chronic exposure to H_2O_2 exerted opposite effects on 3D-HTMCs depending on the culture conditions; in fact, a marked and significant increase of PARP-1 cleavage levels was detected only in 3D-HTMCs static cultures, while in dynamic models 3D-HTMCs PARP-1 expression got a full length.

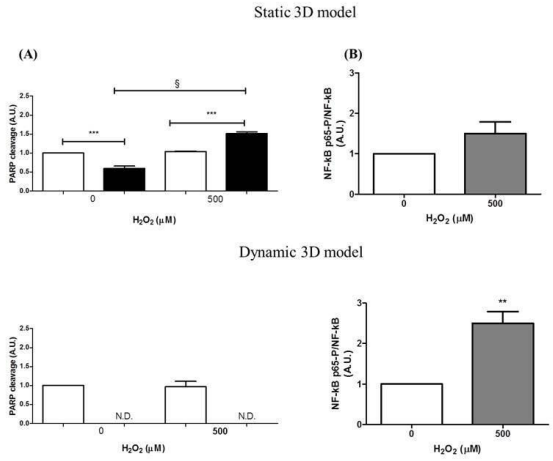

Fig. 5: PARP1 cleaved levels and NF-kB levels in 3D- HTMC static and dynamic cultures after 168hrs of chronic oxidative treatment
The analysis was performed by immunoblotting and the bars represent both the ratio of cleaved PARP1 and phosfoNF-kBp65/NF-kB, and are expressed as arbitrary units (AU). Data represent the mean ± SD of 2 independent experiments, running in triplicate.
*** p <0.0001; **p<0.01 vs. untreated 3D cultures and §p<0.0001 3D-HTMC treated vs 3D-HTMC control cultures (Two-way ANOVA).

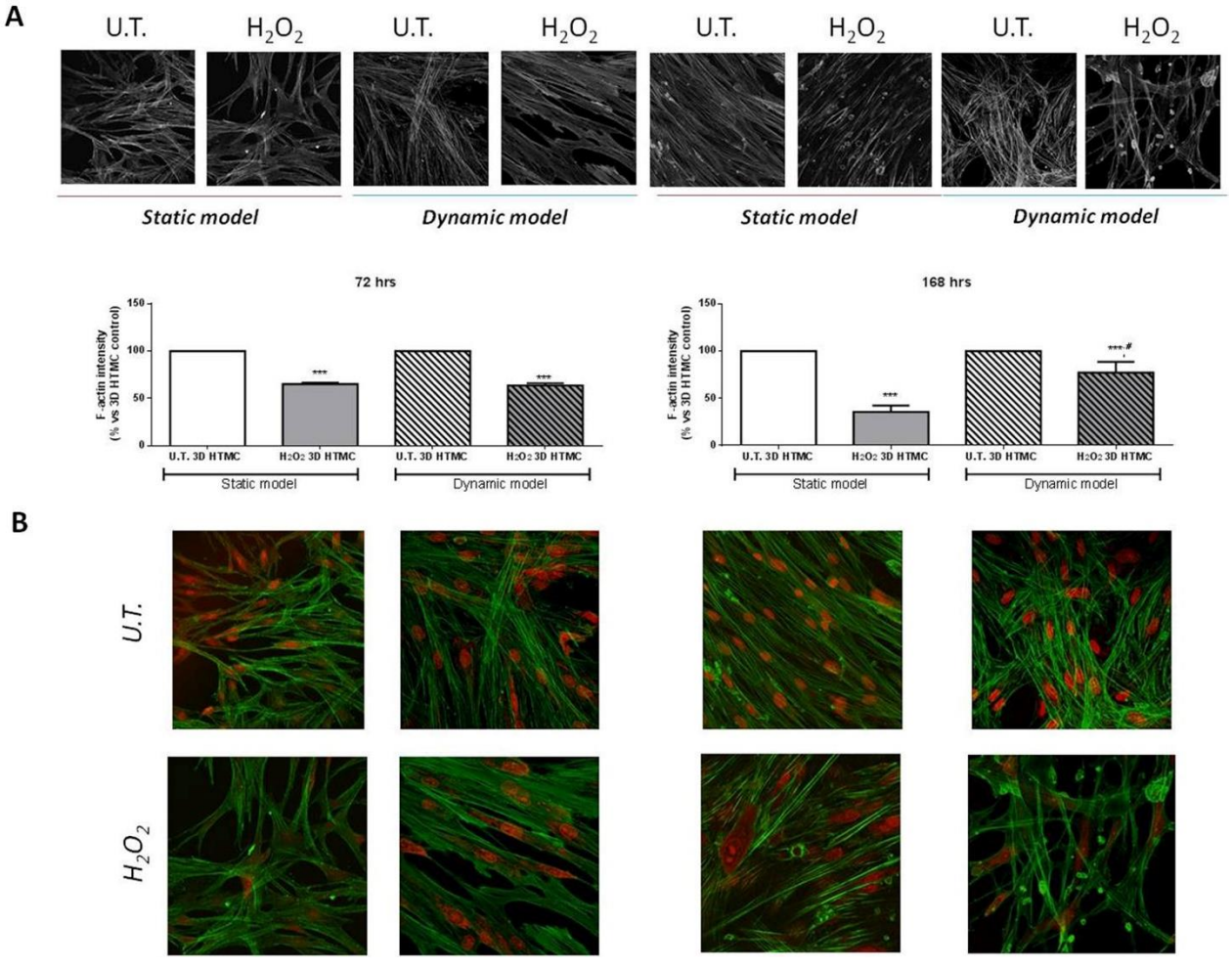

Fig. 6: F-actin intensity measurement and confocal analysis
(A) F-actin intensity was calculated at least into three images of the same condition. Each measurement included ten areas of interest per image. Data represent the mean ± SD of 6 independent experiments. (B) Confocal microscopy analyses of nucleus and cytoskeletal markers were performed on U.T. and H_2O_2- 3D-HTMCs in static and in dynamic conditions after 72 and 168 hours of experimental procedures. Representative images are related to immunoreactivity for To-Pro™ and Phalloidin, as nuclear and cytoskeleton markers, respectively. Merged images showed cytoskeleton plus Nucleus. Fluorescence signals were captured at 60x magnification. *** p <0.0001 vs. U.T. 3D HTMCs and #p<0.05 dynamic H_2O_2 3D-HTMC vs static H_2O_2 3D-HTMC (One-way ANOVA followed by Bonferroni's posttest).

NF-kB transactivation, as an inflammatory / antiapoptotic response marker, was analyzed in terms of the ratio between the levels of phospho-NF-kB p65, the activated form of NF-kB, versus total NF-kB (Figure 4B). A remarkable NF-kB activation occurred only in 3D-HTMC cultured in dynamic conditions.

3.5 Confocal analysis

To understand the dynamics of F-actin in 3D-HTMC under both static and dynamic conditions, during multiple 2 hrs-exposure to 500μM H_2O_2, the F-actin intensity associated with the cytoskeleton was quantified by Fuji ImageJ open source image processing software (Fig. 6, panel A). Therefore, at 72 hrs of experimental procedure, in both culture models a reduction by about 40% in F-actin intensity was observed compared to that of untreated 3D-HTMCs. However, at 168 hrs only in the treated dynamic 3D-HTMC model the F-actin intensity showed a recovery, while in the static 3D-HTMC model F-actin intensity was further reduced by about 64% and 42%, compared to untreated static 3D-HTMC and treated dynamic 3D-HTMC, respectively.

Moreover, the spatial organization of 3D-HTMCs cultures at 72 and 168 hrs was analyzed by confocal microscopy (Fig. 6, panel B). In 3D- static HTMC cultures, the actin microfilaments, detected by fluorescent probe FITC-Phallodin, resulted uniformly distributed in parallel lines along with the longitudinal axis and a lot of cell-to-cell interaction was detected. However, in dynamic 3D-HTMCs, actin microfilaments showed less orderly distribution of the cells embedded in the matrix. In both culture conditions, the H_2O_2- treated 3D-HTMCs showed an increase of nuclear size, labeled by fluorescent probe To-Pro™, while actin microfilament became thicker, tense and distributed in radial manner only in dynamic conditions.

4 Discussion

The aim of the study was to develop a relevant 3D in vitro model of HTMC using Matrigel® and bioreactor technologies to explore, in a more physiological way, the first step of molecular changes in h-TM cultures after prolonged oxidative stress condition.

As known, there are several inducible glaucoma animal models that allow to evaluate the ganglion cell axon damage through the experimental increase of IOP or direct damage of the optic nerve (Burgoyne, 2015; Ishikawa et al., 2015; Struebing and Geisert, 2015; Evangelho et al., 2019). However, these approaches could explain only a part of glaucoma molecular mechanisms; in fact, until today, the only clinically modifiable risk factor remains IOP. Moreover, these not species-specific artifacts overestimate, overlooking fundamental issues, and results cannot always be translated to humans. There is therefore a pressing need for translational value of human biology-based advanced models to understand disease in humans, at multiple biological scales, according to Adverse Outcome Pathway constructs.

In the last few years, 3D-cultures together with 3D-culture techniques have represented important, increasingly physiologically relevant and useful steps towards in vitro models for disease species-specific studies. In particular, the addition of a perfusion flow ranging from milli- to micro-fluidic techniques have implemented the performance of standard 3D-cultures. Indeed, (Ucciferri et al., 2014; Ahluwalia, 2017) reported that cells and tissues cultured in vitro, under specific conditions, maintain power law metabolic scaling in cultures proving the physiological relevance for these downscaled in vitro systems.

In the small dimension-bioreactor scenario, cell-culture chambers, characterized only by a few ml in volume (i.e. "milli-fluidic" chambers), meet specifications to refine animal models allowing for an easy interaction by laboratory experts. As known, the millifluidic apparatus simulates physiological environmental conditions, exposing cells to a cell-culture flow, which acts as blood in the human circulation (Giusti et al., 2014). However, in order to implement the standard static culture method, it is possible to mimic different dynamic environmental conditions, using a peristaltic pump. In this way, cells can affect their habitat and interact with each other, secreting cytokines, and mimicking a real live situation.

In our and other previous studies (Bouchemi et al., 2017; Vernazza et al., 2019) it was given evidence of the suitability of 3D- HTM cultures for assessing a more realistic model than a 2D-model.
In this regard, to further improve our 3D-HTMC in vitro we applied the millifluidic technique to 3D HTMC culture. To assess the effectiveness of this approach, we compared the different biological responses of 3D-HTMCs cultured in a static environment and 3D-HTMC cultured within the flow perfusion bioreactor, during prolonged chronic oxidative stimulus, that is considered closely linked both to TM pathological changes and glaucoma (Saccà and Izzotti, 2014; Zhao et al., 2016).

The benchmarks for the emergence of an aqueous humor outflow resistance are ascribed to cytoskeleton reorganization, cell shape, contractile properties, cell-to-cell/ECM attachments (Xiang et al., 2010). Thus we analyzed 3D-HTMCs morphology by confocal microscopy after repeated 2 hrs-exposures to 500μM H_2O_2 (Fig. 6). The F-actin was chosen as cytoskeleton indicator because it resulted abundant in TM cells. In our experimental conditions, after 72 and 168 hrs exposures to an oxidative stressor, in both 3D-HTMCs culture models, actin microfilaments appeared thinned and nuclear size resulted enlarged compared to that of untreated cultures. These morphological changes confirmed that prolonged OS can modify the TM cells shape (i.e. F-actin cytoskeleton reorganization) through gene expression changes, besides biomechanical insults (Saccà et al., 2016b).

Moreover, also the reduction of F-actin intensity during the short-term doses of H_2O_2 (72 hrs) showed the same trend. As known, the actin cytoskeleton depolymerization is one of the ROS mechanisms by which cell barrier functions may be impaired (Boardman et al., 2004). However, after long-term of H_2O_2 exposure (168 hrs), only treated 3D-HTMC under dynamic conditions showed an increase of F-actin intensity, compared to the previous condition. It could be related to the constant medium nutrients supply, provided by the bioreactor system, that allowed for F-actin recovery (Stapulionis et al., 1997).

Moreover, the amplification of IL1α, IL1β, IL6, TNFα and TGFβ, by qPCR was investigated. After 48hrs of experimental stress condition only in 3D-dynamic HTMC cultures we found a significant up-regulation of TGF-β1 and IL-1β, two crucial markers involved both in ECM remodeling (Pulliero et al., 2014; Lv et al., 2017) and in glaucoma acute inflammatory response (Taurone et al., 2015; Wang et al., 2017). The ECM changes in the TM play an important role in increasing both aqueous humor outflow resistance and IOP (Fig. 3, panel A). Indeed, several molecular factors interact with one another to promote the ECM synthesis or its degradation changing its basic properties (Fuchshofer and Tamm, 2009). Therefore, the MMP, COL1A1 and FN1 gene amplifications were also evaluated and the results indicated that only in 3D-dynamic HTMC, the H_2O_2 exposure could change the expression of cellular proteases in order to counteract OS-induced outflow resistance (Micheal et al., 2013; Singh et al., 2015). However, the adhesion

molecule expressions did not show significant differences compared to the UT 3D HTMC models, even though 3D- HTMC subjected to oxidative stress and cultured under dynamic conditions showed a significant COL1A1 up-regulation ($p<0.01$) compared to treated 3D-HTMC under static conditions. These results highlight that more physiological culture conditions are able to better mimic the homeostatic TM cell responses found in vivo to adjust the outflow resistance (Wang et al., 2001; Acott and Kelley, 2008). Thus, it is conceivable that our model mimics in vivo conditions found in early stages of glaucoma.

In this study we also provided the evidence that 3D-models, compared to the standard 2D cultures commonly used for *in vitro* glaucoma studies, maintained the tissue architecture which represents an important hallmark for the tissue function maintenance found in vivo. However, a dynamic environment allows a better maintenance of cell structures than static culture conditions, also confirmed by confocal analysis, and this capability better supported the cellular polarization, sustaining, as a consequence, a long-term viability of the cells. Indeed, the modulation of apoptosis markers and NF-kB protein levels in 3D- dynamic HTMC cultures showed a more efficient adaptive response over time to OS-damage, compared to 3D-static models (Zahir and Weaver, 2004), triggered the inflammation cascade, as it happens in vivo during glaucoma occurrence.

Then, in 3D-dynamic HTMCs we observed an increase in pro apoptotic proteins including BAD, BIM, BID, and cytochrome C only in early time of pro-oxidant stimulus exposure and a gradual increase over time in TNFα, Tumor Necrosis Factor receptor 1 (TNFR1). However, a stronger increase at 168hrs in anti-apoptotic markers, as survivin and IGFPB1 and in a way also the cell proliferation activator, TNFR2, was found to counterbalance the apoptotic response (Fig. 4). Moreover, these results together with the uncleaved PARP1, the increase of phosfoNF-kBp65 rate compared to total NF-kB level and the healthy metabolic state were in favour of cell survival rather than apoptosis (Fig. 5).

On the other hand, 3D- static HTMC cultures evidenced an overexpression of BAD, BID and Caspase 3 and, to a lesser extent, also of TNRF1, as well as a marked induction of anti-apoptotic proteins such as BCL2, BCLw, survivin, x IAP, CD 40 and IGF1 up to 72hrs of OS-exposure. Nevertheless, after 168hrs to prolonged sub-toxic stress exposure, we reported PARP1 cleaved, no activation of NF-kB and a reduced metabolic cell state leading to hypothesize that 3D-static HTMCs carried on to apoptosis pathway (Figs. 4,5) (Elmore, 2007; Vanamee and Faustman, 2017).

In conclusion, dynamic 3D-HTMCs culture models allow for cellular function preservation over time. These features enable the cells to last prolonged stress attack, and this is what is requested by a relevant *in vitro* model. Indeed, glaucoma is a chronic disease, which shows its effects after long time from the beginning of TM damage. Moreover, this in-vitro biodynamic platform can be further developed to become a useful tool to identify key events of damage onset, and its long-term complications, such as blindness, by mimicking tissue-crosstalk with other tissues, joining different modules/chambers in series. In this way, it is possible to analyze step-by-step the stages of cell damage which underlie glaucoma and its adverse outcomes.

References

Aarskog, N. and Vedeler, C. (2000). Real-time quantitative polymerase chain reaction. *Hum Genet 107*, 494–498. doi:10.1007/s004390000399

Acott, T. S. and Kelley, M. J. (2008). Extracellular matrix in the trabecular meshwork. *Exp Eye Res 86*, 543–561. doi:10.1016/j.exer.2008.01.013

Ahluwalia, A. (2017). Allometric scaling in-vitro. *Sci Rep 7*, 1–7. doi:10.1038/srep42113

Benton, G., Arnaoutova, I., George, J. et al. (2014). Matrigel: From discovery and ECM mimicry to assays and models for cancer research. *Adv Drug Deliv Rev 79–80*, 3–18. doi:10.1016/j.addr.2014.06.005

Berger, E., Magliaro, C., Paczia, N. et al. (2018). Millifluidic culture improves human midbrain organoid vitality and differentiation. *Lab Chip 18*, 3172–3183. doi:10.1039/C8LC00206A

Boardman, K. C., Aryal, A. M., Miller, W. M. et al. (2004). Actin re-distribution in response to hydrogen peroxide in airway epithelial cells. *J Cell Physiol 199*, 57–66. doi:10.1002/jcp.10451

Bouchemi, M., Roubeix, C., Kessal, K. et al. (2017). Effect of benzalkonium chloride on trabecular meshwork cells in a new in vitro 3D trabecular meshwork model for glaucoma. *Toxicol In Vitro 41*, 21–29. doi:10.1016/j.tiv.2017.02.006

Bouhenni, R. A., Dunmire, J., Sewell, A. et al. (2012). Animal models of glaucoma. *J Biomed Biotechnol 2012*, 692609. doi:10.1155/2012/692609

Brancato, V., Gioiella, F., Imparato, G. et al. (2018). 3D breast cancer microtissue reveals the role of tumor microenvironment on the transport and efficacy of free-doxorubicin in vitro. *Acta Biomater*. doi:10.1016/j.actbio.2018.05.055

Burgoyne, C. F. (2015). The Non-Human Primate Experimental Glaucoma Model. *Exp Eye Res 141*, 57–73. doi:10.1016/j.exer.2015.06.005

Elmore, S. (2007). Apoptosis: a review of programmed cell death. *Toxicol Pathol 35*, 495–516. doi:10.1080/01926230701320337

Evangelho, K., Mastronardi, C. A. and de-la-Torre, A. (2019). Experimental Models of Glaucoma: A Powerful Translational Tool for the Future Development of New Therapies for Glaucoma in Humans—A Review of the Literature. *Medicina (Mex) 55*. doi:10.3390/medicina55060280

Fuchshofer, R. and Tamm, E. R. (2009). Modulation of extracellular matrix turnover in the trabecular meshwork. *Exp Eye Res 88*, 683–688. doi:10.1016/j.exer.2009.01.005

Giusti, S., Sbrana, T., La Marca, M. et al. (2014). A novel dual-flow bioreactor simulates increased fluorescein permeability in epithelial tissue barriers. *Biotechnol J 9*, 1175–1184. doi:10.1002/biot.201400004

Gonzalez, J. M., Hamm-Alvarez, S. and Tan, J. C. H. (2013). Analyzing Live Cellularity in the Human Trabecular Meshwork. *Investig Opthalmology Vis Sci 54*, 1039. doi:10.1167/iovs.12-10479

Hughes, C. S., Postovit, L. M. and Lajoie, G. A. (2010). Matrigel: A complex protein mixture required for optimal growth of cell culture. *PROTEOMICS 10*, 1886–1890. doi:10.1002/pmic.200900758

Ishikawa, M., Yoshitomi, T., Zorumski, C. F. et al. (2015). Experimentally Induced Mammalian Models of Glaucoma. *BioMed Res Int 2015*, 281214. doi:10.1155/2015/281214

Izzotti, A., Saccà, S. C., Longobardi, M. et al. (2009). Sensitivity of ocular anterior chamber tissues to oxidative damage and its relevance to the pathogenesis of glaucoma. *Invest Ophthalmol Vis Sci 50*, 5251–5258. doi:10.1167/iovs.09-3871

Kaczara, P., Sarna, T. and Burke, J. M. (2010). Dynamics of H2O2 availability to ARPE-19 cultures in models of oxidative stress. *Free Radic Biol Med 48*, 1064–1070. doi:10.1016/j.freeradbiomed.2010.01.022

Keller, K. E., Bhattacharya, S. K., Borrás, T. et al. (2018). Consensus recommendations for trabecular meshwork cell isolation, characterization and culture. *Exp Eye Res 171*, 164–173. doi:10.1016/j.exer.2018.03.001

Kim, S. H. and Kim, H. (2018). Inhibitory Effect of Astaxanthin on Oxidative Stress-Induced Mitochondrial Dysfunction-A Mini-Review. *Nutrients 10*, 1137. doi:10.3390/nu10091137

Kim, Y. W. and Park, K. H. (2019). Exogenous influences on intraocular pressure. *Br J Ophthalmol*, bjophthalmol-2018-313381. doi:10.1136/bjophthalmol-2018-313381

Kohen, N. T., Little, L. E. and Healy, K. E. (2009). Characterization of Matrigel interfaces during defined human embryonic stem cell culture. *Biointerphases 4*, 69–79. doi:10.1116/1.3274061

Langley, G. R., Adcock, I. M., Busquet, F. et al. (2017). Towards a 21st-century roadmap for biomedical research and drug discovery: consensus report and recommendations. *Drug Discov Today 22*, 327–339. doi:10.1016/j.drudis.2016.10.011

Li, G., Lee, C., Agrahari, V. et al. (2019). In vivo measurement of trabecular meshwork stiffness in a corticosteroid-induced ocular hypertensive mouse model. *Proc Natl Acad Sci 116*, 1714–1722. doi:10.1073/pnas.1814889116

Lv, X., Liu, S. and Hu, Z.-W. (2017). Autophagy-inducing natural compounds: a treasure resource for developing therapeutics against tissue fibrosis. *J Asian Nat Prod Res 19*, 101–108. doi:10.1080/10286020.2017.1279151

Micheal, S., Yousaf, S., Khan, M. I. et al. (2013). Polymorphisms in matrix metalloproteinases MMP1 and MMP9 are associated with primary open-angle and angle closure glaucoma in a Pakistani population. *Mol Vis 19*, 441–447

Osmond, M., Bernier, S. M., Pantcheva, M. B. et al. (2017). Collagen and collagen-chondroitin sulfate scaffolds with uniaxially aligned pores for the biomimetic, three dimensional culture of trabecular meshwork cells. *Biotechnol Bioeng 114*, 915–923. doi:10.1002/bit.26206

Poehlmann, A., Reissig, K., Schönfeld, P. et al. (2013). Repeated H2 O2 exposure drives cell cycle progression in an in vitro model of ulcerative colitis. *J Cell Mol Med 17*, 1619–1631. doi:10.1111/jcmm.12150

Pulliero, A., Seydel, A., Camoirano, A. et al. (2014). Oxidative Damage and Autophagy in the Human Trabecular Meshwork as Related with Ageing. *PLOS ONE 9*, e98106. doi:10.1371/journal.pone.0098106

Saccà, S. C., Corazza, P., Gandolfi, S. et al. (2019). Substances of Interest That Support Glaucoma Therapy. *Nutrients 11*, 239. doi:10.3390/nu11020239

Saccà, S. C., Gandolfi, S., Bagnis, A. et al. (2016a). From DNA damage to functional changes of the trabecular meshwork in aging and glaucoma. *Ageing Res Rev 29*, 26–41. doi:10.1016/j.arr.2016.05.012

Saccà, S. C., Gandolfi, S., Bagnis, A. et al. (2016b). The Outflow Pathway: A Tissue With Morphological and Functional Unity. *J Cell Physiol 231*, 1876–1893. doi:10.1002/jcp.25305

Saccà, S. C. and Izzotti, A. (2014). Focus on molecular events in the anterior chamber leading to glaucoma. *Cell Mol Life Sci CMLS 71*, 2197–2218. doi:10.1007/s00018-013-1493-z

Singh, D., Srivastava, S. K., Chaudhuri, T. K. et al. (2015). Multifaceted role of matrix metalloproteinases (MMPs). *Front Mol Biosci 2*. doi:10.3389/fmolb.2015.00019

Stapulionis, R., Kolli, S. and Deutscher, M. P. (1997). Efficient Mammalian Protein Synthesis Requires an Intact F-Actin System. *J Biol Chem 272*, 24980–24986. doi:10.1074/jbc.272.40.24980

Struebing, F. L. and Geisert, E. E. (2015). What Animal Models Can Tell Us About Glaucoma. In *Progress in Molecular Biology and Translational Science* (365–380). Elsevier. doi:10.1016/bs.pmbts.2015.06.003

Taurone, S., Ripandelli, G., Pacella, E. et al. (2015). Potential regulatory molecules in the human trabecular meshwork of patients with glaucoma: Immunohistochemical profile of a number of inflammatory cytokines. *Mol Med Rep 11*, 1384–1390. doi:10.3892/mmr.2014.2772

Tham, Y.-C., Li, X., Wong, T. Y. et al. (2014). Global Prevalence of Glaucoma and Projections of Glaucoma Burden through 2040: A Systematic Review and Meta-Analysis. *Ophthalmology 121*, 2081–2090. doi:10.1016/j.ophtha.2014.05.013

Ucciferri, N., Sbrana, T. and Ahluwalia, A. (2014). Allometric Scaling and Cell Ratios in Multi-Organ in vitro Models of Human Metabolism. *Front Bioeng Biotechnol 2*. doi:10.3389/fbioe.2014.00074

Vanamee, É. S. and Faustman, D. L. (2017). TNFR2: A Novel Target for Cancer Immunotherapy. *Trends Mol Med 23*, 1037–1046. doi:10.1016/j.molmed.2017.09.007

Vandesompele, J., De Preter, K., Pattyn, F. et al. (2002). Accurate normalization of real-time quantitative RT-PCR data by geometric averaging of multiple internal control genes. *Genome Biol 3*, research0034.1. doi:10.1186/gb-2002-3-7-research0034

Vernazza, S., Tirendi, S., Scarfì, S. et al. (2019). 2D- and 3D-cultures of human trabecular meshwork cells: A preliminary assessment of an in vitro model for glaucoma study. *PLOS ONE 14*, e0221942-. doi:10.1371/journal.pone.0221942

Waduthanthri, K. D., He, Y., Montemagno, C. et al. (2019). An injectable peptide hydrogel for reconstruction of the human trabecular meshwork. *Acta Biomater 100*, 244–254. doi:10.1016/j.actbio.2019.09.032

Wang, J., Harris, A., Prendes, M. A. et al. (2017). Targeting Transforming Growth Factor-β Signaling in Primary Open-Angle Glaucoma: *J Glaucoma 26*, 390–395. doi:10.1097/IJG.0000000000000627

Wang, N., Chintala, S. K., Fini, M. E. et al. (2001). Activation of a tissue-specific stress response in the aqueous outflow pathway of the eye defines the glaucoma disease phenotype. *Nat Med 7*, 304. doi:10.1038/85446

Xiang, Y., Li, B., Li, G.-G. et al. (2010). Effects of endothelin-1 on the cytoskeleton protein F-actin of human trabecular meshwork cells in vitro. *Int J Ophthalmol 3*, 61–63. doi:10.3980/j.issn.2222-3959.2010.01.14

Zahir, N. and Weaver, V. M. (2004). Death in the third dimension: apoptosis regulation and tissue architecture. *Curr Opin Genet Dev 14*, 71–80. doi:10.1016/j.gde.2003.12.005

Zhao, J., Wang, S., Zhong, W. et al. (2016). Oxidative stress in the trabecular meshwork (Review). *Int J Mol Med 38*, 995–1002. doi:10.3892/ijmm.2016.2714

Conflict of interest

The authors declare that they have no conflicts of interest.

Acknowledgments

Dr. Francesco Oddone and Dr. Stefania Vernazza were supported by the Italian Ministry of Health and by Fondazione Roma, Rome, Italy. This work was funded by the award “Omikron Italia 2017 - Marco Centofanti Neuroprotection and Glaucoma”, Omikron srl, Rome, Italy.

We would like to express our gratitude to Ilaria Rizzato, University of Genoa, for revising the English of this paper and to IVTech srl for their technical supporting information.